Direct measurements of conventional and anisotropic magnetocaloric effect in binary RAl_2 single crystals

J. C. B. Monteiro[a] and F. G. Gandra
Universidade Estadual de Campinas, Instituto de Fisica Gleb Wataghin, Campinas, SP 13083-859, Brazil

(Received 18 April 2017; accepted 22 May 2017; published online 5 June 2017)

We report on specific heat and magnetocaloric effect (MCE) measurements in single crystals of $HoAl_2$, $DyAl_2$, and $TbAl_2$ measured by a heat flux technique using Peltier devices. Those compounds order ferromagnetically at 31 K, 61 K, and 106 K respectively, and present a spin reorientation transition (SRT) below T_C. We study the dependence of the SRT with magnetic field and temperature by means of specific heat measurements performed in single crystals oriented at the [100], [110], and [111] directions with the aid of calculations using a simple model. We obtained the conventional MCE for $HoAl_2$ and $TbAl_2$ and also the anisotropic version of the effect obtained indirectly from the specific heat for $TbAl_2$ and $DyAl_2$. We also present the results for a direct determination of the anisotropic MCE for $DyAl_2$ by measuring the heat flux generated by a rotation of the single crystal under constant field. *Published by AIP Publishing.*
[http://dx.doi.org/10.1063/1.4984917]

I. INTRODUCTION

In the past decade, several results[1–9] regarding the Anisotropic Magnetocaloric Effect (AMCE) have attracted attention due to the new perspective it could offer to the magnetic refrigeration research field. The use of magnetic anisotropy as a generator of a temperature change appeared at the end of the 80s when Babkin and Urinov[10] published results on thin films of nickel and Fe_2O_3. The main idea was to trigger the effect by a change in the sample orientation within a fixed magnetic field rather than by a change of the field intensity itself. As their results did not reach good numbers, the AMCE only caught real attention in 2007 when von Ranke *et al.*[11] suggested the possibility of using crystal field effects such as spin reorientation transitions (SRTs) or magnetocrystalline anisotropy as AMCE generators. After that, many others studies have explored anisotropy effects such as metamagnetic transitions,[3,8,12] spontaneous and field induced SRT,[2,5] and shape-anisotropy,[1] as possible AMCE generators. In their study, von Ranke *et al.*[11] presented calculations for the $DyAl_2$ compound, achieving values of $-\Delta S_M = 12.9$ J/kg K for a fixed magnetic field of $\mu_0 H = 1.5$ T, by rotating the field from the easy magnetization direction [100] to a non-easy $[00\bar{1}]$ direction. Patiño *et al.*[2] also reported an expressive result for $HoAl_2$, where calculations predicted an AMCE around 23 J/kg K by rotating the field from the [100] to the [110] crystal direction.

The magnetic properties of the RAl_2 family have been widely studied among the years. In 1990, Purwins and Leson[13] reviewed the main magnetic properties in single crystals of the RAl_2 family, showing a comparison between experimental and theoretical results. With the exception of the antiferromagnetic $CeAl_2$ all the remaining RAl_2 family orders ferromagnetically and many compounds present some anomaly in their magnetization curves. Those anomalies are changes in the direction of the magnetization vector which occurs in order to minimize the energy of the system. They can be interpreted as a competition between energy terms such as anisotropy, thermal oscillations and Zeeman Effect that acts within the system. As the system magnetization rearranges, a corresponding variation of magnetic entropy generates the so-called AMCE. So, the general idea is to exploit the spontaneous or field induced changes in single crystals, which generate the AMCE, and compare to the regular magnetocaloric effect (MCE).

In this study, we use a heat flux technique, associated with temperature and magnetic field sweep protocols, to perform direct measurements of specific heat, conventional and anisotropic MCE in oriented single crystals of $HoAl_2$, $DyAl_2$, and $TbAl_2$. We use simulations constructed with a simple Hamiltonian using the electric crystal field theory and molecular mean field approximation to support the experimental data which are compared to results previously reported in the literature.

II. EXPERIMENTAL

High purity rare earth (99.9%) and aluminum (99.99%) were used to prepare polycrystalline bulks of RAl_2 (R = Tb, Dy, and Ho) in a conventional arc furnace under an argon atmosphere. As the prepared bulks were massive (around 15 g each), they were melt several times to ensure good homogeneity to the sample. Those bulks were taken to a Centorr tri-arc furnace assembly where single crystals of RAl_2 were grown by the Czochralski method.

The growth process is not difficult, and as a reference value, the average growth speed used was about 6 ± 1 mm/h. Cylinder shaped single crystals up to 30 mm long with diameter up to 7 mm were obtained and were cut with a diamond saw into smaller cylinder pieces measuring 5 mm long, which were oriented in the [111], [110], and [100] directions. For the $DyAl_2$ sample, one extra single crystal had the [001]

[a]Electronic mail: jolmiui@gmail.com

axis and $(1\bar{1}0)$ plane identified in order to properly perform the direct rotation experiment. All samples were single phase, and the Laue patterns showed good quality of the single crystals.

To obtain the specific heat and conventional magnetocaloric effect data, we made heat flux measurements with the magnetic field oriented along the [111], [110], and [100] crystal directions using a Quantum Design PPMS (Physical Property Measurement System) with a customized puck built with a Peltier element, as described elsewhere.[14,15] In order to perform the rotating experiment we used a Peltier element mounted on a cold finger cryostat that allows rotation of the crystal inside the bore of an electro-magnet. A Lake Shore Cernox (CX-1050-BC) and a Pt100 sensor were used to control the temperature of the system with the aid of a 340 Lake Shore temperature controller. The voltage readings were made with a Keithley 182 Sensitive Digital Voltmeter and sent to the main computer station. To control the rotation of the calorimeter, we used a servomotor and an optical encoder (1000 pulses per revolution) coupled to the axis of rotation of the calorimeter.

III. THEORY

To properly describe the magnetic properties of the RAl_2 compounds, we used a very simple model Hamiltonian (1), including the cubic crystalline electrical field (CEF) (2), the exchange and Zeeman interactions (3)

$$\widehat{\mathcal{H}} = \widehat{\mathcal{H}}_{CEF} + \widehat{\mathcal{H}}_{Mag}, \tag{1}$$

where $\widehat{\mathcal{H}}_{CEF}$ is the crystalline electrical field contribution using the point charge model, given in the Lea *et al.*[16] notation by

$$\widehat{\mathcal{H}}_{CEF} = W\left[\frac{X}{F_4}\left(O_4^0 + 5O_4^4\right) + \frac{(1-|X|)}{F_6}\left(O_6^0 - 21O_6^4\right)\right]. \tag{2}$$

In Eq. (2), W gives the CEF energy scale and $X\,(-1 < X < 1)$ gives the relative contribution of the fourth and sixth order factors in terms of the Stevens Equivalent Operators,[17,18] O_n^m. The dimensionless factors F_n are tabulated in Ref. 16. In the Hamiltonian (1), $\widehat{\mathcal{H}}_{Mag}$ is the magnetic part, including the exchange and Zeeman interactions, given by

$$\widehat{\mathcal{H}}_{Mag} = -g_J\mu_B\left(\vec{H} + \lambda\vec{M}\right)\cdot\vec{J}, \tag{3}$$

where λ is the exchange parameter, g_J is the Landé factor, μ_B is the Bohr magneton, and H is the applied magnetic field intensity on a given arbitrary direction forming angles $\alpha, \beta,$ and γ with the cubic crystallographic axes x, y, and z. As the focuses of this work are specific heat measurements in oriented single crystals, it is convenient to write the magnetic Hamiltonian as

$$\begin{aligned}\widehat{\mathcal{H}}_{Mag} = g_J\mu_B[&(H\cos(\alpha) + \lambda M_x)J_x + \left(H\cos(\beta) + \lambda M_y\right)J_y \\ &+ \left(H\cos(\gamma) + \lambda M_z\right)J_z].\end{aligned} \tag{4}$$

The magnetization vector components are given by the mean thermodynamic values of the magnetic moment

$$\vec{M}_n = \langle\vec{\mu}_n\rangle = g\mu_B\frac{\sum_{\mathcal{E}_k}\langle\mathcal{E}_k|\vec{J}_n|\mathcal{E}_k\rangle e^{-\beta\mathcal{E}_k}}{\sum_{\mathcal{E}_k} e^{-\beta\mathcal{E}_k}}. \tag{5}$$

In expression (5), $\mathcal{E}_k$ and $|\mathcal{E}_k\rangle$ are the energy eigenvalues and eigenvectors, respectively, and $\beta = 1/k_BT$. The total magnetization and the magnetization intensity along the field direction are given by

$$|\vec{M}| = \sqrt{M_x{}^2 + M_y{}^2 + M_z{}^2} \tag{6}$$

and

$$|\vec{M}_H| = \cos(\alpha)M_x + \cos(\beta)M_y + \cos(\gamma)M_z. \tag{7}$$

The total heat capacity is obtained by

$$C = C_{Latt} + C_{el} + C_{Mag}, \tag{8}$$

where C_{Latt} is the lattice contribution, calculated using the Debye approximation

$$C_{Latt} = 9Nk_B\left(\frac{T}{\theta_D}\right)^3\int_0^{\theta_D/T}\frac{x^4e^x}{\left(e^x-1\right)^2}dx. \tag{9}$$

C_{el} is the conduction electron contribution, given by the well-known linear expression

$$C_{ele} = \gamma T, \tag{10}$$

where $\gamma = \frac{\pi^2k_B{}^2n}{2\epsilon_f}$ is the Sommerfeld coefficient. The magnetic part of the heat capacity is obtained by evaluating the entropy through the partition function and the mean thermodynamic value of the energy

$$S_{Mag} = k_B\ln\left(\sum_{\mathcal{E}_k} e^{-\beta\mathcal{E}_k}\right) + \frac{1}{T}\frac{\sum_{\mathcal{E}_k}\mathcal{E}_k e^{-\beta\mathcal{E}_k}}{\sum_{\mathcal{E}_k} e^{-\beta\mathcal{E}_k}}, \tag{11}$$

and using the heat capacity relation

$$C_p = T\left(\frac{\partial S}{\partial T}\right)_p. \tag{12}$$

To obtain the magnetocaloric effect, we use expression (11) to calculate the magnetic entropy at different magnetic fields and define the conventional magnetocaloric potential through the isothermal magnetic entropy variation as

$$\begin{aligned}&\Delta S_M\left(T, \Delta H = H_f - H_i, \alpha, \beta, \gamma\right) \\ &\quad = S_f\left(T, H_f, \alpha, \beta, \gamma\right) - S_i(T, H_0, \alpha, \beta, \gamma).\end{aligned} \tag{13}$$

The anisotropic MCE is defined by the difference of the isothermal magnetic entropy between two orientations of the crystal within a fixed magnetic field

$$\begin{aligned}\Delta S_{ani}\begin{pmatrix} & \alpha_i \to \alpha_f \\ T,\ H,\ & \beta_i \to \beta_f \\ & \gamma_i \to \gamma_f \end{pmatrix} &= S_f\left(T, \mathrm{H}, \alpha_f, \beta_f, \gamma_f\right) \\ &\quad - S_i(T, H, \alpha_i, \beta_i, \gamma_i).\end{aligned} \tag{14}$$

TABLE I. Model parameters for the RAl_2 family used for calculations of the specific heat, entropy, and magnetocaloric effect.[2,9,13]

	$TbAl_2$	$DyAl_2$	$HoAl_2$
Curie temperature $[T_C\,(\mathrm{K})]$	107	61	32
Spin reorientation temperature $[T_{SR}\,(\mathrm{K})]$	94	45	21
Crystal field parameters $[W\,(\mathrm{meV})]$	0.0200	−0.0109	0.0174
Crystal field parameters $[X]$	0.90	0.28	−0.33
Exchange parameter $[\lambda\,(T^2/\mathrm{meV})]$	87.069	41.379	22.397
Debye temperature $[\theta_D\,(\mathrm{K})]$	360	345	345
Sommerfeld parameter $\left[\gamma\left(\frac{\mathrm{mJ}}{\mathrm{mol}}\mathrm{K}\right)\right]$	10.0	2.0	5.0

IV. RESULTS AND DISCUSSION

The model parameters used to calculate the RAl_2 specific heat, entropy, and magnetocaloric effect quantities are given in Table I. Previous studies already explored the magnetization data of those compounds;[19,20] therefore, in this paper, we focus on the analysis of the calorimetry and magnetocaloric data of single crystals. The entire RAl_2 family presents a second order ferromagnetic (FM) transition and some of them also develop an order-order spin reorientation transition (SRT) at lower temperatures. These SRT are characterized by a change in the easy axis of magnetization, and they are highly dependent on both the applied magnetic field and the temperature. In the following, we show specific heat calculations and experimental data together with conventional and anisotropic MCE results of the $DyAl_2$, $TbAl_2$, and $HoAl_2$, discussing the influence on the SRT.

A. $HoAl_2$

From previous studies, it is known that $HoAl_2$ presents a second order ferromagnetic-paramagnetic (FM-PM) transition at $T_C = (32 \pm 2)$ K and a SRT around 20 K that already have been investigated through magnetization,[13,20] magnetic torque measurements,[21] and scattering of polarized neutrons.[22] The SRT of this sample is characterized by a spontaneous change (occurs at zero magnetic field) of the easy magnetization axis from the [110] direction at low temperatures to the [100] direction above 20 K. This spontaneous change of direction is a result of the competition between the anisotropy and thermal energy, acting in a way to minimize the total energy of the system. When we introduce the magnetic field, we have a third term to contribute to the total energy of the system resulting in profound changes at the behavior of the magnetization, specific heat, entropy, and magnetocaloric effect. By using the expressions defined in Sec. III, we calculated the total specific heat when the magnetic field is applied along the [100], [110], and [111] crystallographic directions using the model parameters of Table I. We also obtained experimental data using the Peltier puck assembly with the PPMS, with the field parallel to the [100] and [111] directions. The results are shown in Fig. 1 where we can see a very good agreement between theory and experiment. As expected, we have the FM ordering at 32 K for all directions, evidenced by a second order λ-type transition, in both calculated and measured curves. We also observe a very well defined SRT, appearing as a sharp peak at $T_{SR} = 21$ K in the $\mu_0 H = 0$ curves (a sharp peak in the Peltier voltage at this temperature indicates that the reorientation has a first order character). In the cases where the magnetic field is parallel to the [111] and [100] directions, the SRT maintains its first order character and shifts towards lower temperature values, when the field intensity is increased. On the other hand, for $\mu_0\vec{H} \parallel [110]$, we can see that a field of 1 T is sufficient to suppress the SRT.

The behavior of the SRT shown in the specific heat curves can be better understood if we look at the magnetization data at different magnetic fields. Figure 2 shows the isofield magnetization curves calculated for the three crystallographic directions of $HoAl_2$. Each set of curves presents the Cartesian projections of the magnetization along the x, y, and z directions. As the [110] direction is the easy one at low temperatures, we can see that at zero applied magnetic field, both the

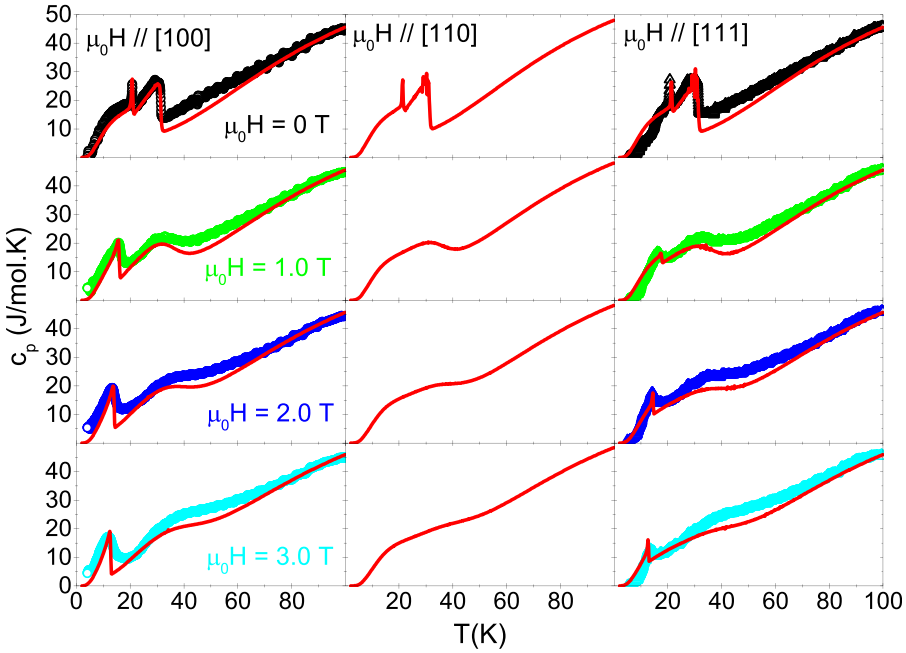

FIG. 1. Specific heat curves calculated (red lines) and measured (colored dots) for $HoAl_2$ single-crystals at magnetic fields up to 3 T.

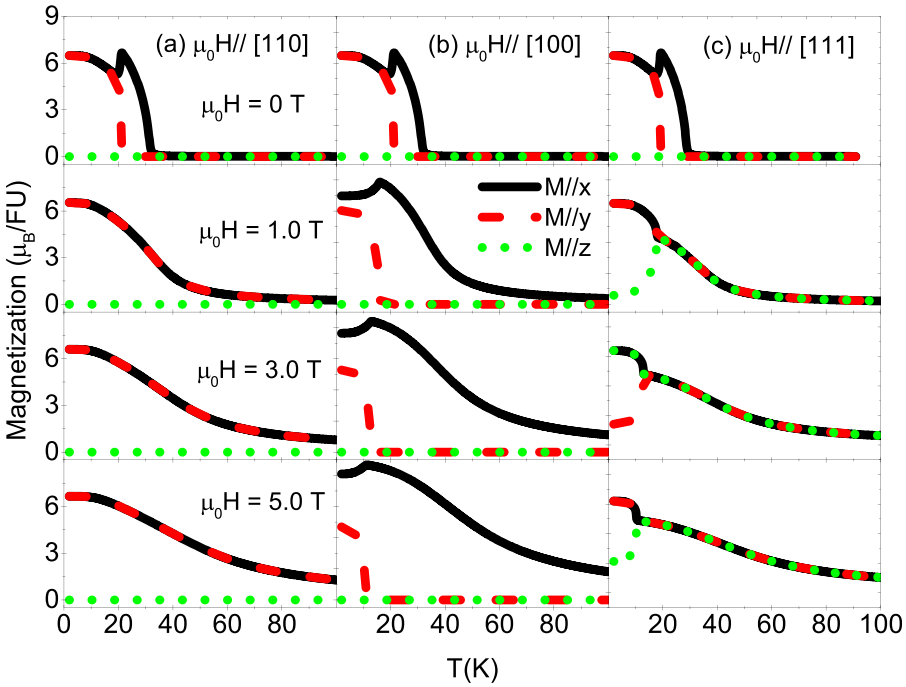

FIG. 2. Calculations of the three Cartesian components of the magnetization of $HoAl_2$ compound for the (a) $\mu_0\vec{H} \parallel [110]$, (b) $\mu_0\vec{H} \parallel [100]$, and (c) $\mu_0\vec{H} \parallel [111]$ cases.

components M_x and M_y, have the same intensity and the M_z component is null. As the temperature rises to T_{SR}, the M_x component value is enhanced and M_y falls to zero, indicating that the magnetization easy axis lies now at the [100] direction. However, in the presence of a magnetic field, this SRT is suppressed, and the easy axis is fixed at the [110] direction. This is in agreement with the specific heat curves where the sharp SRT peak at 21 K disappears for magnetic fields above 0.1 T (verified in our simulations). On the other hand, when the magnetic field is applied parallel to the [111] or [100] directions, we notice that at low temperatures the magnetization components aligned to the field are enhanced and the spin reorientation happens, fully aligning the magnetization to the field direction at T_{RS}, which is reduced as the magnetic field increases.

De Oliveira *et al.*[23] predicted that the magnetic entropy variation of $HoAl_2$ when a magnetic field is applied parallel to the [100] direction would have an inverted peak in the vicinity of the SRT, followed by the conventional peak caused by the FM-PM transition at T_C. We made direct heat flux measurements with the Peltier element assembly, following an already stablished field sweep protocol,[15] and the results agreed very well with our calculated curves, as can be seen in Fig. 3. The results show a giant MCE at T_C, reaching values of 27 J/kg K and a reasonable inverted effect of 9 J/kg K at the SRT, with a magnetic field variation of 5 T.

B. $TbAl_2$

Previous studies[13,24–26] showed that $TbAl_2$ is a simple ferromagnet with $T_C = 105$ K which is the highest Curie temperature among the compounds studied in this paper. In Fig. 4, we show specific heat curves measured by the heat flux technique obtained with $TbAl_2$ single crystals oriented along [100], [110], and [111] directions. At zero magnetic field, we only observe a second order transition at the Curie temperature, so this compound does not suffer any spontaneous SRT opposed to the case of $HoAl_2$. It is known[13] that [111] is the easy magnetization direction for $TbAl_2$, and in this case, the compound seems to behave like a common ferromagnet presenting no other anomalies in the specific heat curves. On the other hand, when the magnetic field is applied out of the easy axis, an anomaly appears on the specific heat data. In the [110] curves, it is very subtle, but in the [100] case, it clearly appears as a λ-type transition below T_C. This anomaly is due to a field-induced spin reorientation where a strong enough magnetic field is capable of turning the magnetization direction from the easy [111] direction to its own. The field-induced SRT of $TbAl_2$ has a second order character and shifts towards lower temperatures as the field is increased. The red lines in Fig. 4

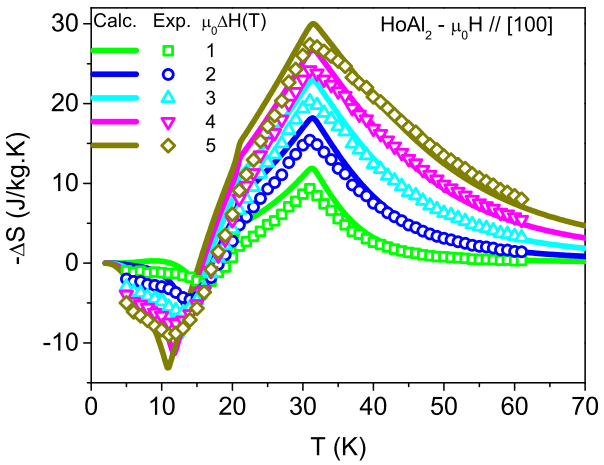

FIG. 3. Magnetocaloric effect of a $HoAl_2$ single crystal with the magnetic field applied parallel to the [100] crystallographic direction. The experimental data (dots) were directly measured with a heat flux technique through the field sweep protocol. The lines show the calculated variation of magnetic entropy using the model Hamiltonian proposed in Sec. III.

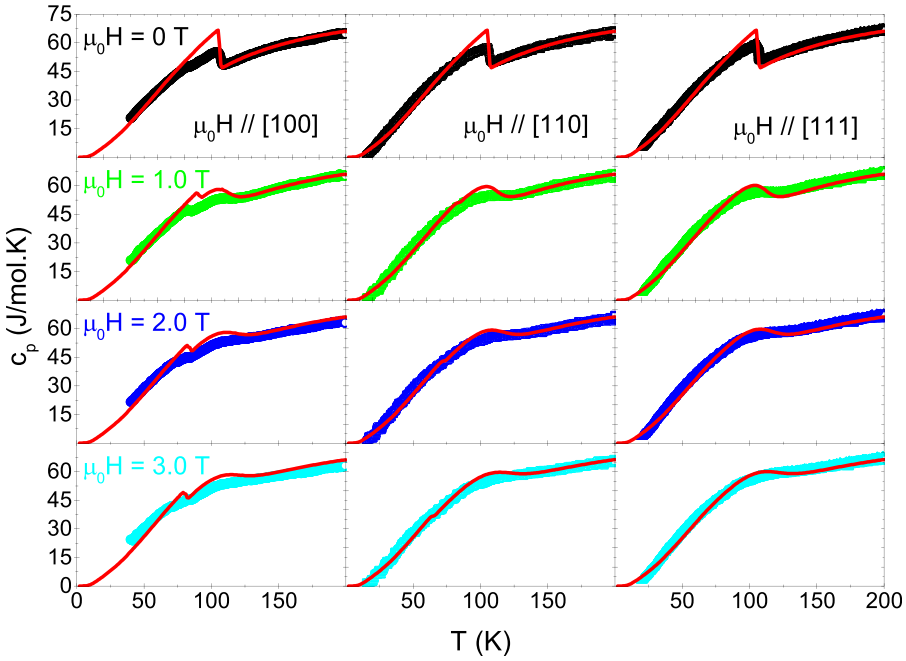

FIG. 4. Specific heat curves measured and calculated for $TbAl_2$ single crystals in situations where the magnetic field was applied parallel to the [100], [110], and [111] directions.

are the calculated curves for the $TbAl_2$, showing that the proposed model agrees with the experimental data.

In Fig. 5, we show the magnetization components simulated for $TbAl_2$ in each of the three discussed directions. We see that at zero applied magnetic field $M_x = M_y = M_z$ indicating that the magnetization remains in the [111] direction. When a magnetic field is applied in the [100] or [110] direction, we can see that as the temperature rises, $\vec{M}$ moves toward the magnetic field direction.

The spin reorientation process that occurs in $TbAl_2$, although subtle compared to the $HoAl_2$ compound, will have some influence on the magnetic entropy variation at low temperatures. The ΔS_M arising from order-order transitions (like the SRT) presents an inverse signal compared to the usual magnetic entropy variation obtained from order-disorder (FM-PM transitions) ones. So, it is expected that the ΔS_M of $TbAl_2$ when $\mu_0\vec{H} \parallel [111]$ should exhibit a broader peak than the $\mu_0\vec{H} \parallel [100]$ case, because of the inverted effect that will arise around T_{SR} in the last one. In Fig. 6, we show the magnetic entropy variation for $TbAl_2$ single crystals measured using the Peltier heat flux technique sweeping the magnetic field. We can clearly see the effect of the SRT by observing the curves at the temperature range between 50 K and 90 K for the $\mu_0\vec{H} \parallel [100]$ and $\mu_0\vec{H} \parallel [111]$ cases. In the former, the ΔS_M decreases much more abruptly at temperatures below T_C, even reaching negative values around 60 K, while in the latter, the entropy variation presents a very broad aspect with an intensity of more than 50% of the peak value at the same

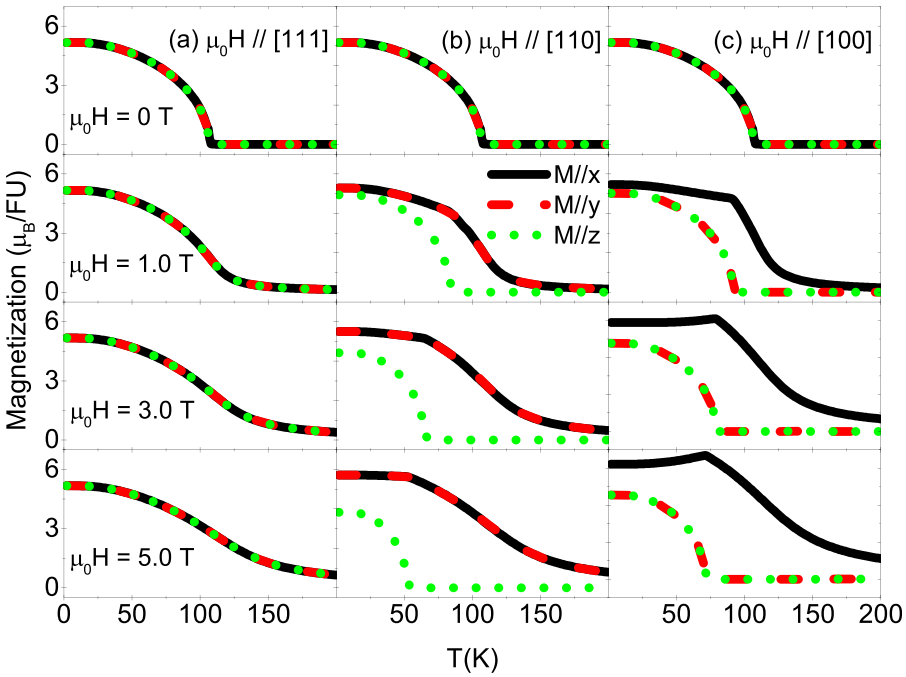

FIG. 5. Simulated magnetization curves for $TbAl_2$. Each Cartesian component is shown for the cases where (a) $\mu_0\vec{H} \parallel [111]$, (b) $\mu_0\vec{H} \parallel [110]$, and (c) $\mu_0\vec{H} \parallel [100]$. One can clearly observe that at zero magnetic field the easy axis of magnetization is the [111] and when a field is applied a field induced SRT occurs, rotating the $\vec{M}$ towards its direction.

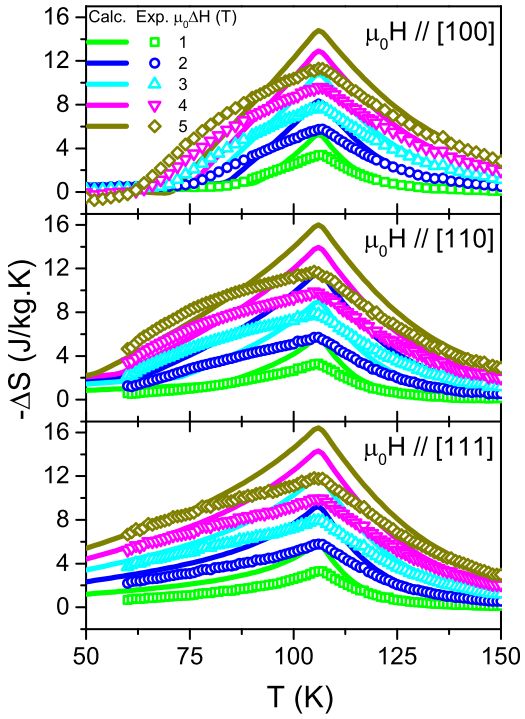

FIG. 6. Conventional MCE obtained both experimentally (dots) and theoretically (lines) for $TbAl_2$ single crystals in three different orientations. The SRT influence can be clearly seen in the range between 50 and 75 K where the ΔS_M rapidly falls to zero at the $\mu_0\vec{H} \parallel [100]$ situation and keeps around 43% of the peak value at the easy direction, $\mu_0\vec{H} \parallel [111]$.

60 K. Under a 5 T magnetic field variation, the difference in terms of the relative cooling power, defined as[27]

$$RCP = \Delta S_{Max} * \Delta T_{fwhm} \tag{15}$$

goes from 587 J/kg, for the $\mu_0\vec{H} \parallel [100]$ experiment, to 837 J/kg for the $\mu_0\vec{H} \parallel [111]$ (ΔT_{fwhm} is the temperature full width at half maximum of the ΔS curve). An increase of 43% caused only by the compound anisotropy and the field induced SRT. The lines represent the calculations using the Hamiltonian proposed and although the theory shows an enhanced peak at T_C compared to the experiment, the overall behavior is very similar between both sets of curves.

The difference arising from the SRT can be explored and used to generate the magnetocaloric effect by using the magnetic anisotropy of the system as the source of variation of magnetic entropy. In Fig. 7, we obtained the anisotropic

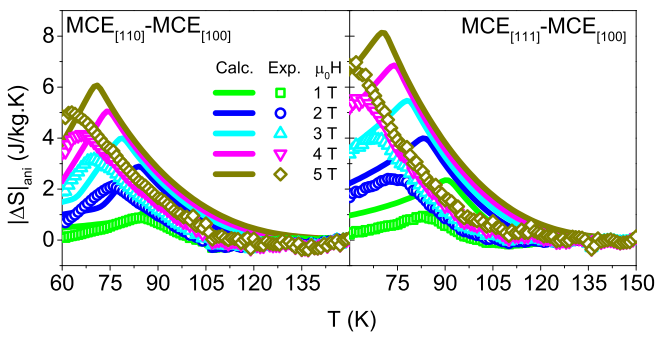

FIG. 7. Anisotropic magnetocaloric effect of $TbAl_2$ obtained indirectly by subtraction of the ΔS_M of the [100], [111], and [110] directions.

MCE by subtracting two sets of curves of a specific direction. We see that the peak of the AMCE appears around the T_{SR}, as expected, and it is strongly field dependent, shifting to lower temperatures as the magnetic field is increased. Exploring the situation where the field is rotated from the [100] direction towards the [111], one can achieve values of 2.4 J/kg K at $\mu_0\Delta H = 2$ T around 74 K and 6.9 J/kg K at $\mu_0\Delta H = 5$ T around 61 K. The difference between the experimental and calculated sets of curves arises mainly due to minor misalignment of the single crystals during the experiment, sample inhomogeneity, and the simplicity of the mathematical model.

C. $DyAl_2$

Following the RAl_2 family behavior, $DyAl_2$ is also a ferromagnetic compound with $T_C = 61$ K. It is also well known that it suffers a SRT below 45 K, as shown by both magnetization[13] and calorimetry measurements.[28] In Fig. 8, we show specific heat results comparing curves obtained by the heat flux technique and simulations made with the proposed Hamiltonian. In agreement with literature results, our data show the easy magnetization direction of $DyAl_2$ to be the [100] direction where a SRT is absent. Both [111] and [110] cases present an anomaly at the specific heat curves when there is an applied magnetic field, as a result of the jump that occurs in the magnetization from the easy direction to the field direction. It is interesting to note that for $\mu_0\vec{H} \parallel [110]$, the SRT keeps the second order character for all applied magnetic fields, but in the $\mu_0\vec{H} \parallel [111]$ case, the Peltier element voltage seems to indicate that at a high field it acquires a first order character.

As the conventional magnetocaloric effect for $DyAl_2$ was already explored in literature,[11,28] here we show the

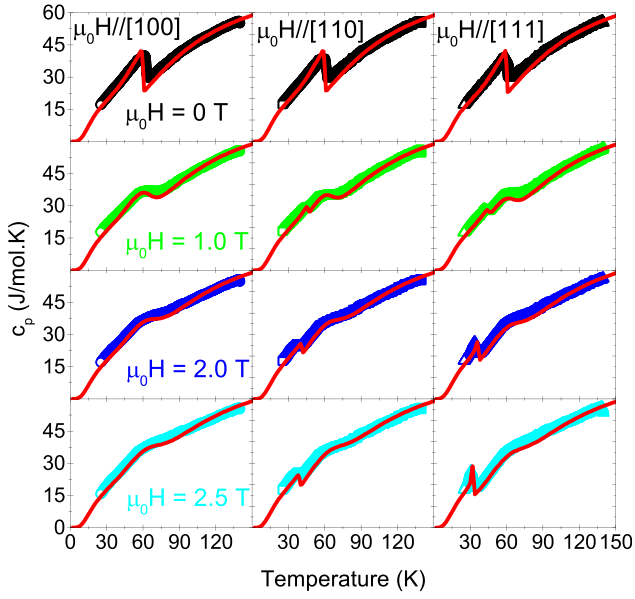

FIG. 8. $DyAl_2$ single crystal specific heat curves measured by the heat flux technique with the Peltier setup. At zero magnetic field, we observe the ferromagnetic transition at 61 K and no SRT. Similar to the $TbAl_2$ behavior, when the field is applied in a direction other than the [100] easy direction, a field induced SRT occurs, resulting from the reorientation of the magnetization from the easy direction to the field direction.

anisotropic MCE for this compound, obtained in the same way as for $TbAl_2$, by subtracting the sets of curves of the conventional variation of magnetic entropy. In Fig. 9, we present the results comparing this indirect experimental method with the calculations, where we can see a very good agreement between the theory and experiment. The AMCE of $DyAl_2$ reaches its highest value in the hypothetical case where one rotates the magnetic field from the [111] direction towards the [100] direction, with a peak of 11.8 J/kg K around 30 K and a RCP of 200 J/kg for a magnetic field variation of 3 T. For comparison, the conventional MCE for $DyAl_2$ with the field applied along the easy [100] direction reaches 14.7 J/kg K around 62 K with a RCP of 617 J/kg for the same $\mu_0\Delta H = 3$ T. While the peak values have a difference of 20%, the RCP of the conventional MCE is about three times bigger than that of AMCE, meaning that the temperature range of the latter is much more limited. Although presenting a reduced MCE potential, the AMCE, it is still interesting because it occurs in a different temperature range and it can be used to improve the performance of a magnetic refrigeration cycle by tuning from one effect to the other in the appropriate temperature range.

The methodology usually adopted in publications regarding the anisotropic magnetocaloric effect[3,6,9] comprises of the difference of two entropy change curves obtained at a fixed magnetic field orientation, just as illustrated earlier. By using the Peltier system, we were able to perform direct AMCE experiments in a single crystal of $DyAl_2$ and measure the total heat flux generated by rotating the sample at constant field and temperature. Figure 10 shows the oriented single crystal glued to the Peltier element. The flat side of the crystal glued to the Peltier corresponds to the $(1\bar{1}0)$ plane and the [001] axis was the starting orientation of the crystal parallel to the magnetic field direction inside the electromagnet. Our experiment was limited to a rotation of 80°, due to space limitations inside the electromagnet gap, and to a magnetic field of 1.9 T.

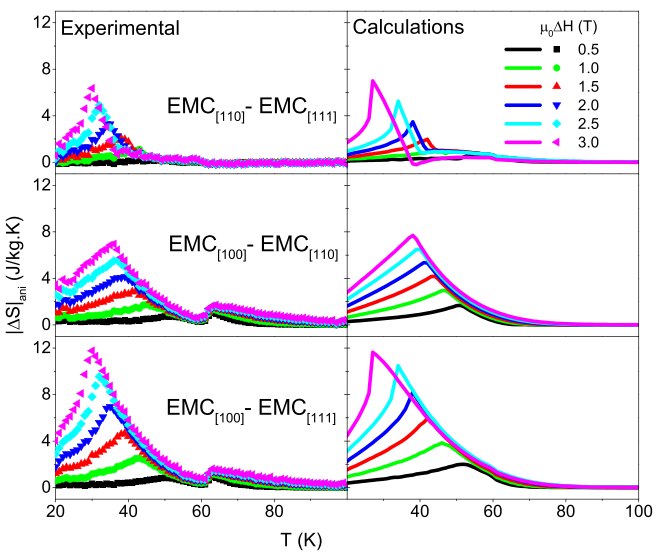

FIG. 9. AMCE of $DyAl_2$ single crystal obtained through subtraction of conventional MCE curves measured through direct heat flux experiments with the Peltier setup. The lines represent calculations of the AMCE with the proposed Hamiltonian. The best scenario was obtained by hypothetically turning the sample between the [111] and [100] directions where we achieved a peak in the ΔS_{aniso} of 11.8 J/kg K for a magnetic field variation of 3 T.

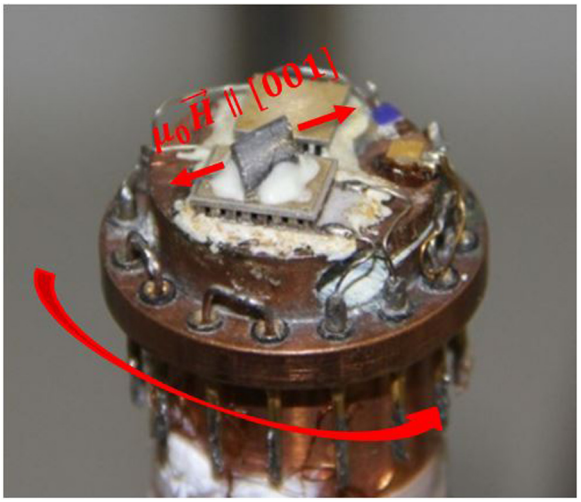

FIG. 10. $DyAl_2$ single crystal properly mounted on the Peltier device used to perform the rotation experiment. The anisotropic magnetocaloric effect was obtained by rotating the calorimeter inside the gap of an electromagnet and measuring the heat flux through the Peltier element.

Because of the angle limitation of the equipment, we show the results of the experiment rotating the crystal from the [001] direction to the [111] direction. In Fig. 11, we show the results where we performed a rotation of about 55°, and the green (filled triangles) and red (filled circles) represent the clockwise and anticlockwise rotation experiments. First, we cooled the sample down to 20 K, at the zero magnetic field. At 20 K, we turned the field on to the desired value and, with both the magnetic field and temperature stabilized, the system makes the rotation of the sample. Between the clock and anticlockwise rotation, we wait for the system to stabilize and the Peltier signal to return to zero. After this, with the magnetic field still on, we go to the next measurement temperature and repeat the process. We compared the results of the direct measurement with those obtained by the subtraction method (filled squares) obtaining the definitive proof that the method really works and can give appreciable results only by rotating the sample inside a constant field. Both methods give almost the same variation of magnetic

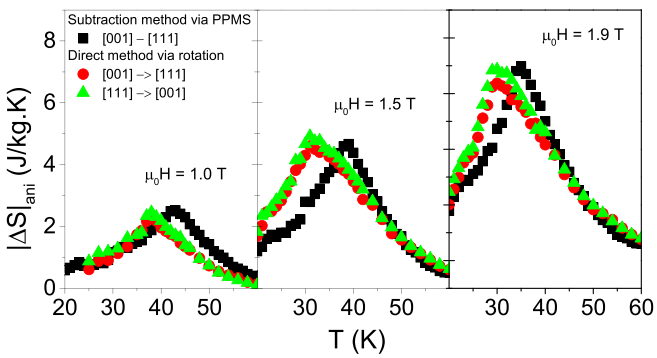

FIG. 11. Direct measurement of the anisotropic magnetocaloric effect of a $DyAl_2$ single crystal through a rotation experiment. The green triangles and red circles represent the clock and anticlockwise rotations, and the black squares are the results of the subtraction method obtained in Fig. 10.

TABLE II. Main results regarding the MCE and AMCE of the RAl_2 compounds studied in this work compared with recent literature results and classical materials. T_{peak} is the peak temperature of ΔS_M, and RCP is the relative cooling power.

		−ΔS (J/kg K)			RCP (J/kg)			
Material	T_{peak} (K)	1 T	2 T	5 T	1 T	2 T	5 T	References
$DyAl_2$ ([100])	61	5.4	9.9	…	118.1	397.3	…	This work
$DyAl_2$ ([100]→[111])	42 (1 T) 35 (2 T)	3.1	7.3	…	74.6	172.0	…	This work
$TbAl_2$ ([111])	106	3.3	5.8	11.8	90.4	281.3	837.8	This work
$TbAl_2$ ([111]→[100])	84 (1 T) 74 (2 T) 61 (5 T)	0.9	2.4	6.9	20.7	84	317.4	This work
$HoAl_2$ ([100])	31	9.3	15.4	27.4	102.3	251.0	980.9	This work
$HoAl_2$ (Theory [110]→[100])	16 (1 T) 14 (2 T) 11 (5 T)	8.9	14.3	23.2	53.4	105.8	229.7	This work
$GdAl_2$	167	…	4.1	7.5	…	267.6	769.3	29
$Gd_5Ge_2Si_2$	272 (1 T) 274 (2 T) 280 (5 T)	1.5	8.2	14.2	13.0	73.9	351.2	15
Gd	294	2.7	4.9	9.3	57.0	180.8	524.5	15
$Fe_{49}Rh_{51}$	313	12.0[a]	15.3	…	127.2	263.7	…	30
Gd_3Ru	54 (1 T) 56 (2 T) 58 (5 T)	15.9	22.4	29.4	65.2	208.3	696.0	31
EuS	18.2	13.0	21.5	36.6	120.7	280.1	767.9	32
PrSi (AMCE)[b] ([100]→[010])	52	6.7	10.8	18.6	55.3	118.9	323.8	33
$ErGa_2$ (AMCE)	5 (5 T)	…	…	6.0	…	…	35	3
$HoGa_2$ (AMCE)	8 (5 T)	…	…	10.5	…	…	73.5	3
$TbMnO_3$ (AMCE)	10	0.4	2.6	11.3	8.7	33.2	200.2	7
DyNiSi (AMCE)[b]	8.8	2.8	11.1	17.5	26.0	142.2	406	1

[a]For a magnetic field variation of 1.25 T.
[b]Calculated through reference data.

entropy achieving values of 7 J/kg K considering a magnetic field of 1.9 T, with peak temperatures separated 5 K apart. Among the possible causes of this temperature difference, we can name a small difference between the temperature of the system and the sample and possible errors in the crystal orientation during the experiments.

V. CONCLUSIONS

In this study, we presented a set of calorimetric and magnetocaloric data obtained for single crystals of $DyAl_2$, $HoAl_2$, and $TbAl_2$ measured by a heat flux technique using Peltier devices as heat flux sensors. In Table II, we compare the main magnetocaloric results obtained in this work with recent studies for well-stablished materials. In general, our results show a good agreement between the experiment and theory using a simple Hamiltonian. For $HoAl_2$, the giant MCE is accompanied by an inverted MCE due to the SRT just as initially predicted by de Oliveira *et al.* For $TbAl_2$, different orientations of the magnetic field relative to the crystal can alter the width of the conventional ΔS curve although keeping the height and peak temperature to the maximum. The AMCE for both $TbAl_2$ and $DyAl_2$ shows a highly field dependent peak temperature (ΔT_{peak} of 15 K between 1 T and 3 T effects) reaching values of 4 J/kg K ($TbAl_2$ [100] ↔ [111]) and 12 J/kg K ($DyAl_2$ [110] ↔ [111]) for a field variation of 3 T. The rotating sample experiment using a 1.9 T field provided an entropy change of 7 J/kg K at 32 K, quite close to the subtraction method. Therefore, the direct experiment is a definitive proof that the magnetic anisotropy can be regarded as an alternative magnetocaloric potential generator for practical purposes.

The final numbers show that AMCE is a viable alternative for refrigerating purposes as it could be implemented together with the conventional effect to better the performance of refrigerating devices. As for $HoAl_2$, we are currently working on alternatives to properly obtain its AMCE as it is a very promising candidate to reach liquid helium temperatures.

ACKNOWLEDGMENTS

We would like to thank the financial support from the Brazilian agencies FAPESP, Capes, CNPq, and FAEPEX-Unicamp.

[1]H. Zhang, Y. Li, E. Liu, Y. Ke, J. Jin, Y. Long, and B. Shen, Sci. Rep. **5**, 11929 (2015).
[2]J. Caro Patiño and N. A. de Oliveira, Intermetallics **64**, 59 (2015).
[3]R. D. dos Reis, L. M. da Silva, A. O. dos Santos, A. M. N. Medina, L. P. Cardoso, and F. C. G. Gandra, J. Alloys Compd. **582**, 461 (2014).
[4]M. Balli, S. Jandl, P. Fournier, and M. M. Gospodinov, Appl. Phys. Lett. **104**, 232402 (2014).
[5]K. P. Skokov, Y. G. Pastushenkov, Y. S. Koshkid'ko, G. Shütz, D. Goll, T. I. Ivanova, S. A. Nikitin, E. M. Semenova, and A. V. Petrenko, J. Magn. Magn. Mater. **323**, 447 (2011).

[6]M. S. Kim, N. H. Sung, Y. Son, M. S. Ko, and B. K. Cho, Appl. Phys. Lett. **98**, 172509 (2011).
[7]J. Jin, X. Zhang, G. Li, Z. Cheng, L. Zheng, and Y. Lu, Phys. Rev. B **83**, 184431 (2011).
[8]D. X. Li, S. Nimori, and T. Shikama, Solid State Commun. **150**, 1865 (2010).
[9]P. J. von Ranke, N. A. de Oliveira, E. J. R. Plaza, V. S. R. de Sousa, B. P. Alho, A. M. G. Carvalho, S. Gama, and M. S. Reis, J. Appl. Phys. **104**, 93906 (2008).
[10]E. V. Babkin and K. O. Urinov, Sov. Phys. J. **32**, 899 (1989).
[11]P. von Ranke, N. de Oliveira, D. Garcia, V. de Sousa, V. de Souza, A. Carvalho, S. Gama, and M. Reis, Phys. Rev. B **75**, 184420 (2007).
[12]D. X. Li, T. Yamamura, S. Nimori, Y. Homma, F. Honda, and D. Aoki, Appl. Phys. Lett. **102**, 152409 (2013).
[13]H. Purwins and A. Leson, Adv. Phys. **39**, 309 (1990).
[14]J. C. B. Monteiro, R. D. dos Reis, F. C. G. Gandra, and N. R. Dilley, Quantum Des. Appl. Notes **1085–200**, 1 (2014); available at http://www.qdusa.com/sitedocs/appNotes/ppms/1085-200.pdf.
[15]J. C. B. Monteiro, R. D. dos Reis, A. M. Mansanares, and F. G. Gandra, Appl. Phys. Lett. **105**, 74104 (2014).
[16]K. R. Lea, M. J. M. Leask, and W. P. Wolf, J. Phys. Chem. Solids **23**, 1381 (1962).
[17]M. Hutchings, Solid State Phys. **16**, 227 (1964).
[18]K. W. H. Stevens, Proc. Phys. Soc., Sect. A **65**, 209 (1952).
[19]H.-G. Purwins, E. Walker, B. Barbara, M. F. Rossignol, and P. Bak, J. Phys. C: Solid State Phys. **7**, 3573 (1974).
[20]W. Schelp, A. Leson, W. Drewes, H.-G. Purwins, and H. Grimm, Z. Phys. B: Condens. Matter **51**, 41 (1983).
[21]C. M. Williams, N. C. Koon, and B. N. Das, J. Appl. Phys. **50**, 1669 (1979).
[22]B. Barbara, J. X. Boucherle, M. F. Rossignol, and J. Schweizer, in *Proceedings of Conference on Neutron Scattering*, edited by R. M. Moon (Energy Research and Development Administration, Gatlingburg, 1976), p. 452.
[23]I. G. de Oliveira, D. C. Garcia, and P. J. von Ranke, J. Appl. Phys. **102**, 73907 (2007).
[24]D. P. Rojas, L. F. Barquín, J. R. Fernandez, J. I. Espeso, and J. C. G. Sal, J. Phys.: Conf. Ser. **200**, 72080 (2010).
[25]F. W. Wang, X. X. Zhang, and F. X. Hu, Appl. Phys. Lett. **77**, 1360 (2000).
[26]T. W. Hill, W. E. Wallace, R. S. Craig, and T. Inoue, J. Solid State Chem. **8**, 364 (1973).
[27]K. A. Gschneidner and V. K. Pecharsky, Annu. Rev. Mater. Sci. **30**, 387 (2000).
[28]A. Lima, A. Tsokol, K. Gschneidner, V. Pecharsky, T. Lograsso, and D. Schlagel, Phys. Rev. B **72**, 24403 (2005).
[29]S. Y. Dan'kov, V. V. Ivtchenko, A. M. Tishin, K. A. Gschneidner, and V. K. Pecharsky, in *Advances in Cryogenic Engineering Materials* (Springer US, Boston, MA, 2000), pp. 397–404.
[30]M. P. Annaorazov, K. A. Asatryan, G. Myalikgulyev, S. A. Nikitin, A. M. Tishin, and A. L. Tyurin, Cryogenics **32**, 867 (1992).
[31]J. C. B. Monteiro, R. D. dos Reis, and F. G. Gandra, Appl. Phys. Lett. **106**, 194106 (2015).
[32]D. X. Li, T. Yamamura, S. Nimori, Y. Homma, F. Honda, Y. Haga, and D. Aoki, Solid State Commun. **193**, 6 (2014).
[33]P. K. Das, A. Bhattacharyya, R. Kulkarni, S. K. Dhar, and A. Thamizhavel, Phys. Rev. B. **89**, 134418 (2014).